IEEE Access
Multidisciplinary | Rapid Review | Open Access Journal

Received March 14, 2020, accepted April 2, 2020, date of publication April 9, 2020, date of current version April 22, 2020.

Digital Object Identifier 10.1109/ACCESS.2020.2986790

Postfault Control and Harmonic Current Suppression for a Symmetrical Dual Three-Phase SPMSM Drive Under Single-Phase Open-Circuit Fault

ZHE LIANG, (Student Member, IEEE), DELIANG LIANG, (Senior Member, IEEE), PENG KOU, (Senior Member, IEEE), AND SHAOFENG JIA, (Member, IEEE)

School of Electrical Engineering, Xi'an Jiaotong University, Xi'an 710049, China
State Key Laboratory of Electrical Insulation and Power Equipment, Xi'an Jiaotong University, Xi'an 710049, China

Corresponding author: Deliang Liang (dlliang@mail.xjtu.edu.cn)

This work was supported in part by the National Natural Science Foundation of China (NSFC) under Project 51737010 and Project 51677144, and in part by the State Key Laboratory of Electrical Insulation and Power Equipment under Grant EIPE19109.

ABSTRACT Multiphase machines have been attracting more and more attentions in high-reliability-required applications due to their inherent fault-tolerant capability. Postfault control strategies with-standing open-circuit faults (OCFs) for several multiphase machine types, like five-phase, symmetrical six-phase (S6) and asymmetrical six-phase (A6) machines, have been widely investigated in recent literatures. However, fault-tolerant control for symmetrical dual three-phase (D3) machines have rarely been studied so far. To fill the gap, this paper addresses key issues in postfault decoupling modeling and field orient control (FOC) for the dual three-phase surface-mounted permanent magnet synchronous machine (SPMSM) with isolated neutrals under single-phase OCF. To do so, a postfault decoupling model with reduced-order transformation is established for D3 machines. Postfault current references are reconfigured with two main-stream criteria: minimum-loss (ML) and maximum-torque (MT). Furthermore, third harmonic flux linkage/back-EMF are taken into account in modeling and control, since it causes third harmonic currents and hence torque ripples under single-phase OCF. Proportional-resonant controllers are employed to decrease the third harmonic currents and torque pulsations. The validity of the postfault control strategies is proved by experiments.

INDEX TERMS Dual three-phase, fault-tolerant control, open-circuit fault, permanent-magnet synchronous machine (PMSM).

I. INTRODUCTION

Fault-tolerant capability is one of the outstanding advantages of multiphase machines in comparison with conventional three-phase ones. The utilization of redundant degrees of freedom in multiphase drives provides the possibility of continuous operation in the event of faults. Owing to this inherent merit, multiphase drives have been practically selected as attractive candidates in safety-critical applications, such as aircrafts, electric vehicles, ship propulsion, and high-reliability industrial drives, where uninterrupted operation under faulty conditions is demanded for security and economic reasons [1]–[4].

In order to exploit the fault-tolerance of multiphase drives in presence of faults, recent research studies have been focus on the machine design [5], postfault modeling [6], [7], and control [8]–[10] for various types of multiphase machine drives. Although fault-tolerant capability of five-phase drives has drawn more attention in the recent literature [7], [9]–[11], the $3k$-phase machines, in which the number of phases is divisible by three, are more attractive in industrial applications, due to the fact that widely used three-phase converters are more easy to extended to $3k$-phase drives via parallel connection [12]. Among $3k$-phase machines, six-phase machines have been widely

The associate editor coordinating the review of this manuscript and approving it for publication was Zhuang Xu.

reported in the last decade [3], [4], [8], [13]–[15]. According to the specific spatial shifted angle of 0, $\pi/6$, and $\pi/3$ between two three-phase windings, the generic six-phase machines can be categorized into three mainstream topologies: dual three-phase (D3), asymmetrical six-phase (A6), and symmetrical six-phase (S6) machines, respectively [3], [13], [14]. Because of better air-gap flux distribution, A6 machines are favored over D3 and S6 ones. For this reason, A6 machines are widely investigated in literatures [8], [14], [15]. Though A6 machines are superior to D3 machines in performance, the latter ones are still adopted in some low-cost applications because they can be easily controlled as two individual three-phase machines with the same control algorithm. In some D3 machines with symmetrical winding arrangement, both three-phase winding sets spatially placed in completely symmetrical parts of the stator, the topology is characterized by a high self-inductance and low mutual inductance which allows to limit current in the case of a short circuit and weaken the magnetic coupling between the faulty and healthy phases [16], [17]. Nevertheless, fault-tolerance capability withstanding electrical faults in D3 drives is barely investigated in the past literature, which is studied in this paper.

The main electrical faults in D3 drives are open-circuit fault (OCF) and short-circuit fault (SCF). OCFs are caused by numerous reasons, such as mechanical disconnection between the converter and phase windings, internal winding rupture, and semiconductor component failures. SCFs can come into OCFs by isolating the faulty phase from healthy ones with fast fuses or breakers. For this reason, OCF is the most common fault discussed in previous studies [15], [18]. The fact that one or more OCFs appear in multiphase drives may cause large torque ripples, serious mechanical vibration, and eventual shutdown of the entire drive. Therefore, proper postfault control strategies are strongly demanded to maintain the continuity of operation and acceptable derating performance under faulty conditions.

Several postfault control strategies concerning the multiphase machines under one or more OCFs have been proposed in previous works [7]–[9], [15], [19]. In these studies, the common principle of the postfault control strategies was to maintain the same rotating magnetomotive force (MMF) as in the prefault situation. The simplest postfault control strategy called as redundant control strategy for $3k$-phase machine is to disable and isolate the whole three-phase winding containing the open-circuit phase to maintain the continuity of operation [20], [21]. However, the redundant control naturally causes significant reduction in output power/torque. In order to improve the power/torque density under faulty condition, more suitable postfault control strategies are required. The commonly used method is to readapt the remaining healthy phase currents. In order to achieve an optimal performance in one aspect, the remaining current reference signals are always regenerated by different optimization criteria, such as minimum copper loss (ML) and maximum torque (MT) criteria [15], [22]. Specially, the ML criterion achieves minimum stator copper losses at given torque but limited available torque and unbalanced current amplitude. In contrast, the MT criterion achieves maximum torque with equal current amplitude at cost of higher copper losses. Recently, the full-range ML (FRML) criteria, as a hybrid MLMT combination between the ML and the MT criteria, was presented in [23] and [24] which ensures the minimum losses in the whole torque operation range (TOR). Along with these principles, hysteresis current controllers were typically used to track the reference currents [25]. However, these controllers suffer from drawbacks as high switch loss, large current ripples, and electromagnetic compatibility problem caused by unfixed switching frequency.

In order to overcome the disadvantages of hysteresis controllers, the postfault decoupled FOC with proportional-integral (PI) current regulators has been exploited in advanced drive applications since they demonstrates excellent steady-state and transient performances. However, to improve the postfault performance of FOC under OCFs, the reduced-order model and modified SVPWM suitable for faulty condition are required. Different multiphase machine types and different OCFs lead to various reduced-order transformations. Reduced-order models for five-phase [7], [19] and A6 machines [8], [26] under OCFs have been well-established. Relevant postfault FOC strategies have also been investigated under a variety of scenarios: different winding connection patterns [25], different neutral configurations [8], [22], [27], and the effect of trapezoidal back EMF on postfault performance [7], [9], [25]. Postfault operations under single-phase OCF for S6 [6] or conventional three-phase [28], [29] machines are also discussed. However, the reduced-order decoupled model and corresponding postfault FOC strategy for D3 machines under single-phase OCF are still missing.

Field experiences have demonstrated that the harmonic currents and torque ripples appear when single-phase OCF occurs. Postfault torque ripples are caused by comprehensive effects of the third components of back EMF harmonics and torque-producing component of currents pulsation [7], [11]. Several approaches to suppress the postfault torque-producing current harmonics have been developed, as feed-forward current compensation [10], sliding mode control (SMC) [7], [11], PI-type current control in multiple synchronous frames [30] and proportional-resonant (PR) current controllers [8], [31]. Among these methods, PR controllers are adopted in this paper for postfault harmonic current suppression since they are easy to digitally implement in practice without heavy computational burden.

To address the above issues, this paper develops a postfault FOC strategy for the D3 surface-mounted PMSM (SPMSM) with isolated neutrals under single-phase OCF. A reduced-order transformation is proposed to obtain the postfault decoupled model under arbitrary single-phase OCF. In this decoupled model, the effects of the mutual inductance between D3 windings and the third back

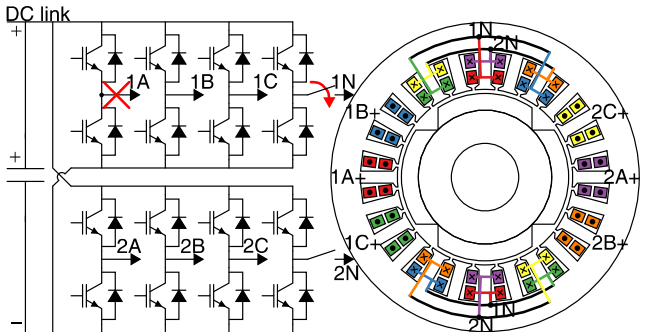

FIGURE 1. The geometry of the 24-slot 4-pole dual three-phase SPMSM and its fault-tolerant inverter topology.

EMF harmonics associated with permanent-magnet (PM) are comprehensively considered. Based on the decoupled model, postfault FOC strategies with two mainstream criteria, i.e., ML FOC and MT FOC, are presented. In order to suppress the postfault third current harmonics, PR controllers are employed in rotating frame. Furthermore, a modified space vector pulse width modulation (SVPWM) is developed for the faulty three-phase VSI. With the above approaches, a complete postfault FOC scheme for D3 SPMSM under single-phase OCF is established.

The rest of this paper is organized as follows. The geometry of the D3 SPMSM and its redundant drive are briefly introduced in Section II. The postfaul model of D3 SPMSM is established in Section III. In Section IV, postfault FOC strategies are presented. Experimental steady-state and dynamic performances are shown in Section V. Conclusions are drawn in Section VI.

II. MACHINE GEOMETRY AND DRIVE CIRCUIT

The winding configuration and drive circuit of a 24-slot 4-pole D3 SPMSM studied in this paper is depicted in Fig. 1. This type includes two sets of three-phase windings (1A, 1B, 1C and 2A, 2B, 2C) independently fed by two IGBT-based 2-level VSIs, which are connected in parallel to a single dc link. Three-phase windings-1 and -2 are individually star-connected and neutrals 1N and 2N are isolated. 1N and 2N are respectively connected to the midpoints of two additional redundant legs via two controllable bidirectional switches (TRIACs or bidirectional IGBT modules). With this configuration, fault-tolerant capability against arbitrary single-phase OCF can be achieved. The redundant VSI for the D3 machine used herein can be regarded as the combination of two redundant VSIs for conventional three-phase drives connected in parallel [29].

III. D3 SPMSM MODEL UNDER SINGLE-PHASE OCF

A. POSTFAULT MODEL IN STATIONARY FRAME

In this paper, the D3 SPMSM model with arbitrary one phase open-circuit is given. For the sake of generality, the case of phase-1A of three-phase winding set-1 open-circuited is studied. Removing the quantities related with phase-1A from the healthy voltage equations, the reduced-order voltage equations of the remaining phases can be expressed as (1). In (1), the mutual inductance between two three-phase windings and the third harmonic back-EMF are taken into account.

$$\mathbf{u}_F = \mathbf{R}_F\mathbf{i}_F + \mathbf{L}_F\frac{d\mathbf{i}_F}{dt} + \omega\left(\lambda_{m1}\begin{bmatrix} -\sin(\theta-\frac{2\pi}{3}) \\ -\sin(\theta+\frac{2\pi}{3}) \\ -\sin\theta \\ -\sin(\theta-\frac{2\pi}{3}) \\ -\sin(\theta+\frac{2\pi}{3}) \end{bmatrix} - 3\lambda_{m3}\begin{bmatrix}1\\1\\1\\1\\1\end{bmatrix}\sin 3\theta\right) \quad (1)$$

where $\mathbf{u}_F = [u_{1b}, u_{1c}, u_{2a}, u_{2b}, u_{2c}]^\top$ and $\mathbf{i}_F = [i_{1b}, i_{1c}, i_{2a}, i_{2b}, i_{2c}]^\top$ are phase voltage and current vectors without phase-1A, respectively; θ is the electrical position of the rotor; ω is the electrical angular velocity; λ_{m1} and λ_{m3} are the fundamental and the third harmonic PM flux linkages, respectively; $\mathbf{R}_F = \text{diag}\,(R_s)_5$, R_s is the phase resistance; $\mathbf{L}_F$ is the remaining submatrix of $\mathbf{L}_{abc}$ with the elements of the row-1A and column-1A removed, $\mathbf{L}_{abc}$ is the inductance matrix. The elements of $\mathbf{L}_F$ can be expressed as

$$L_{1i1j} = L_{2i2j} = \begin{cases} L_{ls}+L_s, & i=j \\ M_s, & i\neq j, \end{cases}$$
$$L_{1i2j} = L_{2i1j} = \begin{cases} L_m, & i=j \\ M_m, & i\neq j \end{cases} \quad (2)$$

In (2), L_{ls} is the leakage inductance, L_s is the main self-inductance, M_s is the mutual inductance in the same winding, L_m is the mutual inductance between the same phases of two three-phase windings, and M_m is the mutual inductance between the different phases of two three-phase windings.

If the magnetic saturation effects are neglected, the electromagnetic torque T_e can be derived by derivating of the magnetic co-energy W'_m with respect to the rotor position θ, i.e., (3) and (4), as shown at the bottom of the next page where n_P is the number of pole pairs.

B. REDUCED-ORDER TRANSFORMATIONS AND DECOUPLED MODEL

Under single-phase OCF, conventional Clarke and Park transformations for D3 machine modeling cannot be used, since the voltage and torque equations are asymmetry. In order to obtain the postfault decoupled model in rotating frame, a set of coordinate transformations listed in (5) is developed. These transformations map vectors into the d–q frame. The principle of transformations is to maintain the fundamental back-EMF under the faulty condition the same as that under the normal condition.

$$\mathbf{Q}_1 = \sqrt{\frac{1}{2}}\begin{bmatrix}-1 & 1\\ -1 & -1\end{bmatrix},\ \mathbf{Q}_1^{-1} = \mathbf{Q}_1^\top,\ \mathbf{D}_1 = \begin{bmatrix}\sqrt{3} & 0\\ 0 & 1\end{bmatrix},$$

$$\mathbf{D}_1^{-1} = \begin{bmatrix} \sqrt{\frac{1}{3}} & 0 \\ 0 & 1 \end{bmatrix}, \ \mathbf{Q}_2 = \sqrt{\frac{2}{3}} \begin{bmatrix} 1 & 0 \\ -\frac{1}{2} & \frac{\sqrt{3}}{2} \\ -\frac{1}{2} & -\frac{\sqrt{3}}{2} \end{bmatrix},$$

$$\mathbf{Q}_2^{\top} = \sqrt{\frac{2}{3}} \begin{bmatrix} 1 & -\frac{1}{2} & -\frac{1}{2} \\ 0 & \frac{\sqrt{3}}{2} & -\frac{\sqrt{3}}{2} \end{bmatrix}, \ \mathbf{R}(\theta_i) = \begin{bmatrix} \cos\theta & \sin\theta \\ -\sin\theta & \cos\theta \end{bmatrix} \tag{5}$$

Using the transformations in (5), the transformations mapping postfault voltage and current vectors from *abc* frame to *d–q* frame can be written as

$$\mathbf{T}_U(\theta) = \begin{bmatrix} \mathbf{R}(\theta)\mathbf{D}_1\mathbf{Q}_1^{\top} & \mathbf{O}_{2,3} \\ \mathbf{O}_{3,2} & \mathbf{R}(\theta)\mathbf{Q}_2^{\top} \end{bmatrix} \tag{6}$$

$$\mathbf{T}_I(\theta) = \begin{bmatrix} \mathbf{R}(\theta)\mathbf{D}_1^{-1}\mathbf{Q}_1^{\top} & \mathbf{O}_{2,3} \\ \mathbf{O}_{3,2} & \mathbf{R}(\theta)\mathbf{Q}_2^{\top} \end{bmatrix} \tag{7}$$

where $\mathbf{T}_U(\theta)$ and $\mathbf{T}_I(\theta)$ are the transformation matrices for voltage and current vectors, respectively. $\mathbf{O}_{2,3}$ and $\mathbf{O}_{3,2}$ are zero matrices with 2×3 and 3×2 zeros, respectively.

By substituting (6) and (7) into (1), the voltage equations in *d–q* frame can be expressed as

$$\begin{aligned} \mathbf{u}_{dq} &= \mathbf{R}_{dq}\mathbf{i}_{dq} + \mathbf{L}_{dq}\frac{d\mathbf{i}_{dq}}{dt} + \omega\mathbf{J}\mathbf{L}_{dq}\mathbf{i}_{dq} \\ &\quad + \omega\sqrt{\frac{3}{2}}\left(\lambda_{m1}\begin{bmatrix} 0 & 1 & 0 & 1 \end{bmatrix}^{\top}\right. \\ &\quad \left. + 3\lambda_{m3}\begin{bmatrix} \sin 2\theta + \sin 4\theta & -\cos 2\theta + \cos 4\theta & 0 & 0 \end{bmatrix}^{\top}\right) \end{aligned} \tag{8}$$

where $\mathbf{u}_{dq} = [u_{1d}, u_{1q}, u_{2d}, u_{2q}]^{\top}$ and $\mathbf{i}_{dq} = [i_{1d}, i_{1q}, i_{2d}, i_{2q}]^{\top}$ are respectively phase voltage and current vectors in *d–q* reference frame under the condition of phase-1*A* open. $\mathbf{R}_{dq} = \mathbf{T}_U(\theta)\mathbf{R}_F\mathbf{T}_I^{-1}(\theta)$, $\mathbf{L}_{dq} = \mathbf{T}_U(\theta)\mathbf{L}_F\mathbf{T}_I^{-1}(\theta)$ and $\mathbf{J} = \left(\mathbf{R}(\theta)\frac{d\mathbf{R}^{-1}(\theta)}{d\theta}\right) \oplus \left(\mathbf{R}(\theta)\frac{d\mathbf{R}^{-1}(\theta)}{d\theta_i}\right)$ can be calculated as

$$\mathbf{R}_{dq} = R_s\mathrm{diag}(3,1,1,1), \quad \mathbf{J} = \begin{bmatrix} 0 & -1 & 0 & 0 \\ 1 & 0 & 0 & 0 \\ 0 & 0 & 0 & -1 \\ 0 & 0 & 1 & 0 \end{bmatrix},$$

$$\mathbf{L}_{dq} = \begin{bmatrix} 3L_{ls}+L & 0 & M & 0 \\ 0 & L_{ls}+L & 0 & M \\ M & 0 & L_{ls}+L & 0 \\ 0 & M & 0 & L_{ls}+L \end{bmatrix} \tag{9}$$

where $L = L_s - L_m$ and $M = M_s - M_m$.

From (9) it can be seen that the inductance matrix $\mathbf{L}_{dq}$ is non-diagonal, which means currents in two *d–q* frame are still coupled. To address this, an additional orthogonal transformation $\mathbf{T}$ is introduced to make $\mathbf{T}\mathbf{L}_{dq}\mathbf{T}^{-1}$ approximately diagonal, that is

$$\mathbf{T} = \frac{\sqrt{2}}{2}\begin{bmatrix} 1 & 0 & 1 & 0 \\ 0 & 1 & 0 & 1 \\ -1 & 0 & 1 & 0 \\ 0 & -1 & 0 & 1 \end{bmatrix}, \quad \mathbf{T}^{-1} = \frac{\sqrt{2}}{2}\begin{bmatrix} 1 & 0 & -1 & 0 \\ 0 & 1 & 0 & -1 \\ 1 & 0 & 1 & 0 \\ 0 & 1 & 0 & 1 \end{bmatrix}. \tag{10}$$

On the other hand, a new reference frame, named as s–e frame in this paper, has been introduced by the transformation $\boldsymbol{T}$. Voltage and current vectors in s–e frame can be expressed as $\boldsymbol{u}_{se} = \boldsymbol{T}\boldsymbol{u}_{dq}$ and $\boldsymbol{i}_{se} = \boldsymbol{T}\boldsymbol{i}_{dq}$, i.e.,

$$\begin{aligned} \begin{bmatrix} u_{sd} \\ u_{sq} \\ u_{ed} \\ u_{eq} \end{bmatrix} &= \frac{\sqrt{2}}{2}\begin{bmatrix} u_{2d}+u_{1d} \\ u_{2q}+u_{1q} \\ u_{2d}-u_{1d} \\ u_{2q}-u_{1q} \end{bmatrix}, \\ \begin{bmatrix} i_{sd} \\ i_{sq} \\ i_{ed} \\ i_{eq} \end{bmatrix} &= \frac{\sqrt{2}}{2}\begin{bmatrix} i_{2d}+i_{1d} \\ i_{2q}+i_{1q} \\ i_{2d}-i_{1d} \\ i_{2q}-i_{1q} \end{bmatrix}. \end{aligned} \tag{11}$$

It can be seen in (11) that all quantities with the subscript "*s*" represent the sum of the quantities of *d–q* frame, whereas all quantities with the subscript "*e*" represent the error of the quantities of *d–q* frame. Applying transformation (10) to all quantities in (8), the voltage equations can be expressed in *s–e* frame as

$$\begin{aligned} \mathbf{u}_{se} &= \mathbf{R}_{se}\mathbf{i}_{se} + \mathbf{L}_{se}\frac{d\mathbf{i}_{se}}{dt} + \omega\mathbf{J}\mathbf{L}_{se}\mathbf{i}_{se} \\ &\quad + \omega\sqrt{3}\left(\lambda_{m1}\begin{bmatrix} 0 \\ 1 \\ 0 \\ 0 \end{bmatrix} + \frac{3}{2}\lambda_{m3}\begin{bmatrix} \sin 2\theta + \sin 4\theta \\ -\cos 2\theta + \cos 4\theta \\ -\sin 2\theta - \sin 4\theta \\ \cos 2\theta - \cos 4\theta \end{bmatrix}\right) \end{aligned} \tag{12}$$

$$\begin{aligned} W'_m &= \frac{1}{2}\mathbf{i}_F^{\top}(\mathbf{L}_F - L_{ls}\mathrm{diag}(1))\mathbf{i}_F + \lambda_{m1}\mathbf{i}_F^{\top} \\ &\quad \cdot \begin{bmatrix} \cos(\theta - \frac{2\pi}{3}) & \cos(\theta + \frac{2\pi}{3}) & \cos\theta & \cos(\theta - \frac{2\pi}{3}) & \cos(\theta + \frac{2\pi}{3}) \end{bmatrix}^{\top} + \lambda_{m3}\mathbf{i}_F^{\top} \cdot \begin{bmatrix} 1 & 1 & 1 & 1 & 1 \end{bmatrix}^{\top} \cos 3\theta \end{aligned} \tag{3}$$

$$\begin{aligned} T_e &= \frac{\partial W'_m}{\partial\theta} = -n_P\lambda_{m1}\mathbf{i}_F^{\top} \\ &\quad \cdot \begin{bmatrix} \sin(\theta - \frac{2\pi}{3}) & \sin(\theta + \frac{2\pi}{3}) & \sin\theta & \sin(\theta - \frac{2\pi}{3}) & \sin(\theta + \frac{2\pi}{3}) \end{bmatrix}^{\top} - 3n_P\lambda_{m3}\mathbf{i}_F^{\top} \cdot \begin{bmatrix} 1 & 1 & 1 & 1 & 1 \end{bmatrix}^{\top} \sin 3\theta \end{aligned} \tag{4}$$

where $\mathbf{R}_{se} = \mathbf{T}\mathbf{R}_{dq}\mathbf{T}^{-1}$, $\mathbf{L}_{se} = \mathbf{T}\mathbf{L}_{dq}\mathbf{T}^{-1}$ are given by (13).

$$\mathbf{R}_{se} = R_s \begin{bmatrix} 2 & 0 & -1 & 0 \\ 0 & 1 & 0 & 0 \\ -1 & 0 & 2 & 0 \\ 0 & 0 & 0 & 1 \end{bmatrix}$$
$$\mathbf{L}_{se} = \begin{bmatrix} 2L_{ls}+L+M & 0 & -L_{ls} & 0 \\ 0 & L_{ls}+L+M & 0 & 0 \\ -L_{ls} & 0 & 2L_{ls}+L-M & 0 \\ 0 & 0 & 0 & L_{ls}+L-M \end{bmatrix} \tag{13}$$

The last term in (12) represents the back-EMF vector in s–e frame, which can be decomposed into two terms as follows,

$$\begin{aligned} \mathbf{E}_{se} &= \mathbf{E}_{se1} + \mathbf{E}_{se3} = \omega(\mathbf{\Lambda}_{se1} + \mathbf{\Lambda}_{se3}) \\ \mathbf{\Lambda}_{se1} &= K_{E1}\begin{bmatrix} 0 & 1 & 0 & 0 \end{bmatrix}^{\top}, \\ \mathbf{\Lambda}_{se3} &= K_{E3}\begin{bmatrix} \sin 2\theta + \sin 4\theta \\ -\cos 2\theta + \cos 4\theta \\ -\sin 2\theta - \sin 4\theta \\ \cos 2\theta - \cos 4\theta \end{bmatrix} \end{aligned} \tag{14}$$

where $K_{E1} = \sqrt{3}\lambda_{m1}$, $K_{E3} = \frac{3}{2}\sqrt{3}\lambda_{m3}$ are the coefficients of the fundamental and third harmonic back-EMF, respectively; $\frac{K_{E3}}{K_{E1}} = \frac{3}{2}\frac{\lambda_{m3}}{\lambda_{m1}}$; $\mathbf{E}_{se}$, $\mathbf{E}_{se1}$, $\mathbf{E}_{se3}$ are the total, fundamental and third harmonic back-EMF vectors in s–e frame, respectively.

From (14) it can be seen that the total back-EMF in s–e frame can be decoupled into two parts: the fundamental back-EMF remains the same as that in normal operation. The pulsating back-EMF, fluctuating at twice and four times of electrical speed in d–q frame, excites third harmonic phase currents.

Substituting (7) and (10) into (4), the electromagnetic torque can be expressed with s–e currents as

$$\begin{aligned} T_e &= T_{e1} + T_{e3} = n_P\mathbf{i}_{se}^{\top}\cdot\mathbf{\Lambda}_{se1} + n_P\mathbf{i}_{se}^{\top}\cdot\mathbf{\Lambda}_{se3}, \\ T_{e1} &= K_{T1}i_{sq}, \quad T_{e3} = K_{T3}\left((i_{sd}-i_{ed})(\sin 2\theta + \sin 4\theta)\right. \\ &\quad \left. + (i_{sq}-i_{eq})(-\cos 2\theta + \cos 4\theta)\right) \end{aligned} \tag{15}$$

where $K_{T1} = n_P K_{E1}$, $K_{T3} = n_P K_{E3}$, T_e represents the total electromagnetic torques, T_{e1} and T_{e3} are the average torque and pulsating torque, respectively.

As seen in (15), the postfault average torque, T_{e1}, is kept as the same as that in normal operation, due to the preservation of back-EMF. However, torque ripples T_{e3} appears after fault due to the interaction between $\mathbf{\Lambda}_{se3}$ and $\mathbf{i}_{se}$. Although both fundamental and third harmonic currents interact with the third harmonic back-EMF resulting in torque ripples, the third harmonic currents bring not only torque ripples but also additional losses. So they have to be suppressed by proper compensation strategy.

From the control point of view, as seen in (12), the voltage equation is nonlinear and can be divided into two parts: the fundamental part and the third harmonic part. The former can be considered as the linear time-invariant system and the latter can be treated as the time-variant disturbances. The voltage equation in s–e frame can be approximately decoupled and expressed as

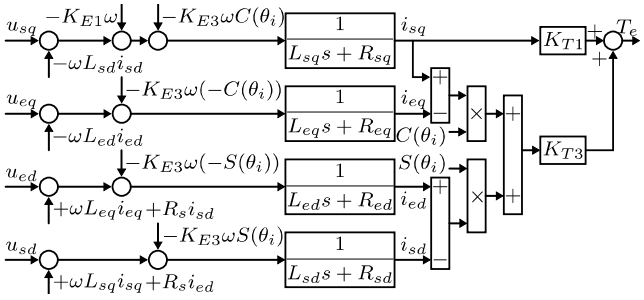

FIGURE 2. Decoupled model in s-e reference frame under single-phase OCF. $C(\theta) = -\cos 2\theta + \cos 4\theta$, $S(\theta) = \sin 2\theta + \sin 4\theta$.

$$(\bar{\mathbf{L}}_{se}\frac{d}{dt} + \bar{\mathbf{R}}_{se})\mathbf{i}_{se} = \mathbf{u}_{se} - \mathbf{E}_{se1} - \underbrace{\mathbf{E}_{se3}}_{\text{disturbance}} - \underbrace{(\omega\mathbf{J}\bar{\mathbf{L}}_{se} + \tilde{\mathbf{R}}_{se})\mathbf{i}_{se}}_{\text{cross-coupling}} \tag{16}$$

where $\bar{\mathbf{L}}_{se}$, $\bar{\mathbf{R}}_{se}$ and $\tilde{\mathbf{R}}_{se}$ are parameters defined in (17).

$$\begin{aligned} \bar{\mathbf{R}}_{se} &\triangleq R_s\mathrm{diag}(2,1,2,1) \triangleq \mathrm{diag}(R_{sd}, R_{sq}, R_{ed}, R_{eq}), \\ \tilde{\mathbf{R}}_{se} &\triangleq \mathbf{R}_{se} - \bar{\mathbf{R}}_{se}, \\ \bar{\mathbf{L}}_{se} &= \mathrm{diag}(2L_{ls}+L+M, L_{ls}+L+M, \\ &\quad 2L_{ls}+L-M, L_{ls}+L-M) \\ &\triangleq \mathrm{diag}(L_{sd}, L_{sq}, L_{ed}, L_{eq}) \end{aligned} \tag{17}$$

Here $\bar{\mathbf{L}}_{se}\frac{d}{dt} + \bar{\mathbf{R}}_{se}$ is diagonal which means the model represented by (16) is decoupled. $\mathbf{E}_{se3}$ and $\left(\omega\mathbf{J}\bar{\mathbf{L}}_{se} + \tilde{R}_{se}\right)\mathbf{i}_{se}$ are treated as disturbance term and cross-coupling term, respectively. It should be noted that the non-diagonal elements, $-L_{ls}$ in (13), are neglected since the leakage inductance is much smaller than self-inductance. The block diagram of decoupled model is shown in Fig. 2.

IV. POSTFAULT FOC CONTROL UNDER SINGLE-PHASE OCF

A. FOC FOR SINGLE-PHASE OCF OPERATION

In variable speed drives, most postfault FOC control schemes based on double closed loops use an outer speed controller to generate the torque reference. According to (15), the postfault average torque T_{e1} is only linear to i_{sq}. Thus, the current reference i_{sq} can directly inherited from the torque reference. However, the other current references, i.e., i_{sd}, i_{ed} and i_{eq}, have to be determined by additional constraints. The popular additional constraints in previous literatures can be categorized in two main principles: minimum loss (ML) criteria and maximum torque (MT) criteria. ML criteria minimizes stator copper losses resulting in unequal magnitudes of phase currents. In contrast, MT criteria forces the equal magnitudes of phase currents.

1) ML FOC

It is well-known that "$i_d = 0$" is required for non-salient machine to achieve maximum torque per ampere (MTPA).

According to (11) and (15), "$i_{1q} + i_{2q} =$ constant" is also required to provide the reference torque. Hence, the minimization problem of instantaneous stator copper losses under single-phase OCF can be expressed in d–q frame as

$$\begin{aligned}\min_{\mathbf{i}_{dq}} p_{\text{copper}} &= \mathbf{i}_{jk}^{\top}\mathbf{R}_{jk}\mathbf{i}_{jk} = \mathbf{i}_{dq}^{\top}\mathbf{R}_{dq}\mathbf{i}_{dq} \\ &= R_s\mathbf{i}_{dq}^{\top}\text{diag}(3,1,1,1)\mathbf{i}_{dq} = R_s(3i_{1d}^2 + i_{1q}^2 + i_{2d}^2 + i_{2q}^2) \\ \text{s.t.}\quad & i_{1d} = i_{2d} = 0, i_{1q} + i_{2q} = \text{constant}. \end{aligned} \tag{18}$$

According to the Cauchy-Schwarz inequality, the optimization condition for (18) is "$i_{1q} = i_{2q}$" in d–q frame, or "$i_{eq} = 0$" in s–e frame. The constraints for ML FOC can be expressed as

$$i_{sd} = i_{ed} = i_{eq} = 0, \quad i_{sq} = \text{constant}. \tag{19}$$

Substituting constraints (19) into (15), the torque expression generated by ML FOC can be simplified as

$$T_e = K_T i_{sq}\left(1 + 1.5\left(\frac{\lambda_{m3}}{\lambda_{m1}}\right)(-\cos 2\theta + \cos 4\theta)\right) \tag{20}$$

2) MT FOC

When MT FOC is employed, the equal current amplitude of the remaining phases is required. Assuming that at steady-state i_{1d} and i_{2d} are kept zero whereas i_{1q} and i_{2q} are kept constant, namely I_{1q} and I_{2q}, respectively. The remaining healthy phase currents in abc frame can be obtained by applying $\mathbf{T}_I^{-1}(\theta)$ in (7), i.e.,

$$\begin{aligned}&\begin{bmatrix} i_{1b} & i_{1c}\end{bmatrix}^{\top} \\ &= \sqrt{\frac{2}{3}}\begin{bmatrix} -\sqrt{3}I_{1q}\sin(\theta - \frac{\pi}{6}) & -\sqrt{3}I_{1q}\sin(\theta + \frac{\pi}{6})\end{bmatrix}^{\top}, \\ &\begin{bmatrix} i_{2a} & i_{2b} & i_{2c}\end{bmatrix}^{\top} \\ &= \sqrt{\frac{2}{3}}\begin{bmatrix} -I_{2q}\sin\theta & -I_{2q}\sin(\theta - \frac{2\pi}{3}) & -I_{2q}\sin(\theta + \frac{2\pi}{3})\end{bmatrix}^{\top}\end{aligned} \tag{21}$$

Note that, as seen in (21), "$\sqrt{3}\ I_{1q} = I_{2q}$" in steady-state, or "$\sqrt{3}\ i_{1q} = i_{2q}$" in transient, is required for equal phase current amplitude. Combining these two constraints, "$i_{1d} = i_{2d} = 0$" which is required for MTPA and "$i_{1q} = i_{2q} =$ constant" which is for the certain torque generation, the constraints for MT FOC are

$$i_{sd} = i_{ed} = 0, \quad i_{sq} = \text{constant}, \ i_{eq} = 0.268 i_{sq}, \tag{22}$$

where $0.268 = \frac{\sqrt{3}-1}{\sqrt{3}+1}$.

Substituting constraints (22) into (15), the torque based on MT FOC can be simplified as

$$T_e = K_T i_{sq}\left(1 + 1.098\left(\frac{\lambda_{m3}}{\lambda_{m1}}\right)(-\cos 2\theta + \cos 4\theta)\right) \tag{23}$$

where $1.098 = \frac{3}{2}(\sqrt{3} - 1)$.

As seen in (20) and (23), even though the condition "$i_{sd} = i_{ed} = 0$" and "$i_{sq} =$ constant" are satisfied, the torque ripples are inevitable with either ML or MT principle, due to the existence of $\lambda_{m3}/\lambda_{m1}$. Besides, i_{sd}, i_{sq}, i_{ed} and i_{eq} are hardly kept constant only with PI controllers due to the existence of $\lambda_{m3}/\lambda_{m1}$. In light of this, it is necessary to design suitable current compensators to suppress the third harmonic phase currents.

B. THIRD HARMONIC CURRENT COMPENSATION

With the forward compensation to cancel the cross-coupling terms in (16), four current controllers are required to regulate the four components of currents in s–e frame. With these controllers, the general closed-loop transfer function of the s–e currents can be uniformly written as

$$\begin{aligned} I_x(s) &= G_{\text{ref}x}(s)I_{\text{ref}x} - G_{E3x}(s)E_{3x}(s) \\ &= \frac{C_x(s)G_{\text{PWM}}(s)G_{LRx}(s)}{1 + C_x(s)G_{\text{PWM}}(s)G_{LRx}(s)}I_{\text{ref}x}(s) \\ &\quad - \frac{G_{LRx}(s)}{1 + C_x(s)G_{\text{PWM}}(s)G_{LRx}(s)}E_{3x}(s), \\ x &= sd, sq, ed, \text{ or } eq \end{aligned} \tag{24}$$

where $G_{\text{ref}x}(s)$ is the closed-loop transfer function from i_x to $i_{\text{ref}x}$, and $G_{E3x}(s)$ is the transfer function from i_x to E_{3x}. $C_x(s)$ is the transfer function of current controller. $C_x(s)\,G_{\text{PWM}}(s)\,G_{LRx}(s)$ is the open-loop transfer function. In an average s-domain model, the PWM converter model can be simplified as a delay unit with the delay period $1.5T_{\text{PWM}}$ and then approximated as

$$G_{\text{PWM}}(s) = \frac{1}{1.5T_{\text{PWM}+1}} \tag{25}$$

where T_{PWM} is the sampling period.

According to internal model principle, to completely suppress a periodic disturbance, an internal model of the periodic disturbance must be included in the controller. From (25), That $|C_x(j\omega_0)| \to \infty$ for the given frequency ω_0 implies that

$$\left|\frac{G_{LRx}(j\omega_0)}{1 + C_x(j\omega_0)G_{\text{PWM}}(j\omega_0)G_{LRx}(j\omega_0)}E_{3x}(j\omega_0)\right| \to 0, \tag{26}$$

which means that the effect of third harmonic back-EMF disturbance E_{3x} is completely eliminated.

In this paper, the PIR controllers for suppressing the given harmonics in s-e current closed-loops is established by connecting two ideal resonant terms in parallel with a PI controller. If the steady-state electrical speed is supposed as ω_0, $\theta_i = \omega_0 t + \theta_0$ where θ_0 is the initial phase. $\mathbf{E}_{se3}$ can be expressed as

$$\mathbf{E}_{se3} = K_{E3}\omega_0\begin{bmatrix} \sin 2(\omega_0 t + \theta_0) + \sin 4(\omega_0 t + \theta_0) \\ -\cos 2(\omega_0 t + \theta_0) + \cos 4(\omega_0 t + \theta_0) \\ -\sin 2(\omega_0 t + \theta_0) - \sin 4(\omega_0 t + \theta_0) \\ \cos 2(\omega_0 t + \theta_0) - \cos 4(\omega_0 t + \theta_0)\end{bmatrix} \tag{27}$$

The components of $\mathbf{E}_{se3}(s)$ in s-domain have different numerators but a common denominator, which is $(s^2 + (2\omega_0)^2)(s^2 + (4\omega_0)^2)$. In order to suppress the disturbance,

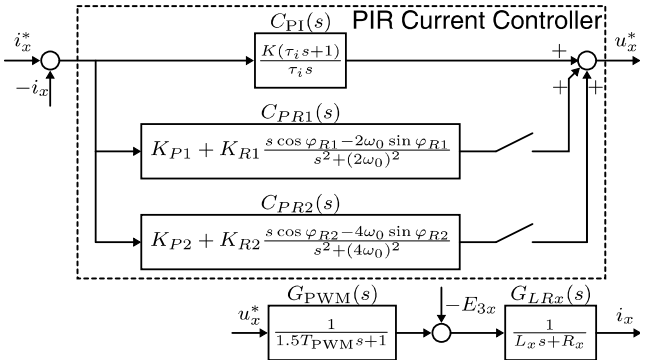

FIGURE 3. The unified block diagram of the *x*-axis current closed-loop.

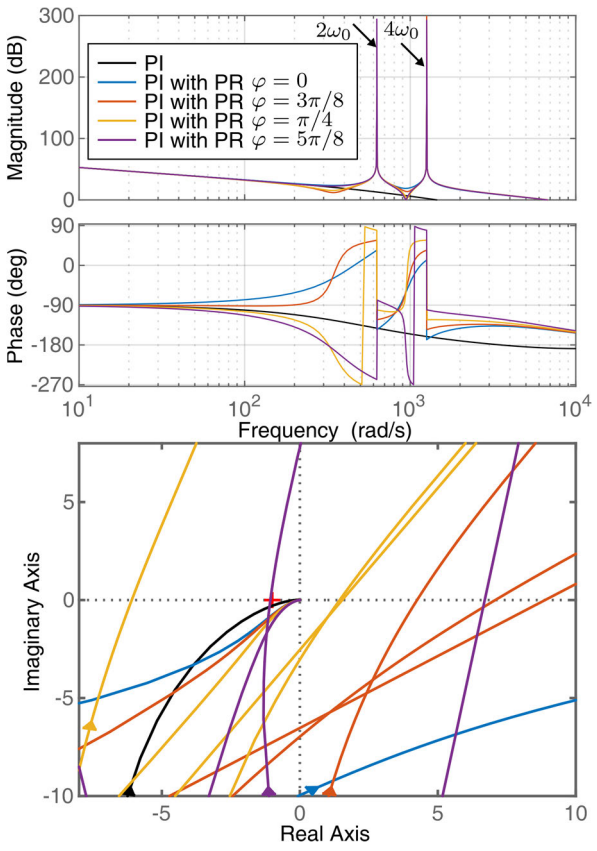

FIGURE 4. Bode plots (top) and Nyquist curves (bottom) of the open-loop transfer functions $C_{PIx}(s)+C_{PR1x}(s)+C_{PR2x}(s)$ with different adjustment angles. The closed-loop system is unstable when $\varphi=\frac{\pi}{4}$ and $\frac{5\pi}{8}$. $\varphi=\frac{3\pi}{8}$ is selected as a trade-off between stability and dynamics.

the resonant frequencies must be set equal to the frequencies of periodic disturbance signal. The basic transfer function of the two resonant terms are

$$C_{PR1}(s)=K_{P1}+K_{R1}\frac{s\cos\varphi_{R1}-2\omega_0\sin\varphi_{R1}}{s^2+(2\omega_0)^2} \tag{28}$$

$$C_{PR2}(s)=K_{P1}+K_{R2}\frac{s\cos\varphi_{R2}-4\omega_0\sin\varphi_{R2}}{s^2+(4\omega_0)^2} \tag{29}$$

where K_{P1} and K_{P2} are the proportional gains, respectively; K_{R1} and K_{R2} are the gains of the 2nd- and 4th-order resonant

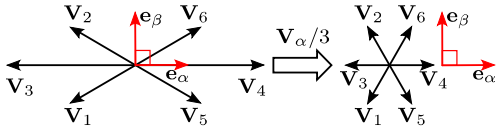

FIGURE 5. Relationship between the postfault and healthy base voltage vectors.

terms, respectively; φ_{R1} and φ_{R2} are the adjustment phases to improve the stability of resonant controller. Finally, the *x*-axis current controller can be expressed as

$$C_x(s)=C_{PI}(s)+C_{PR1x}(s)+C_{PR2x}(s) \tag{30}$$

Fig. 3(a) depicts the closed-loop block diagram of the *x*-axis current. The switches in resonant branches are turn off during dynamics and turn on at the end of dynamics to avoid the side effect and suppress steady-state harmonics. In order to determine the suitable parameters of resonant terms, the determination process proposed in [31] is adopted to determine the parameters in (28) and (29). Fig. 4 shows the bode plots and nyquist curves of the open-loop transfer functions with different parameters.

C. POSTFAULT SVPWM

Under single-phase OCF, the conventional three-phase SVPWM for healthy winding should be modified for the faulty winding. The output voltage vectors of the healthy three-phase VSI driving the three-phase winding set-2 are determined by the switch states (S_{a2}, S_{b2}, S_{c2}). $S_i = 1$ means that the upper switch is on and the lower one is off while $S_i = 0$ means that the upper switch is off and the lower one is on, $i = a2, b2, c2$. The output voltage vector can be expressed in α–β plane using $\mathbf{Q}_2^\top$ in (5), i.e.,

$$\begin{aligned}\begin{bmatrix}u_{\alpha2}\\u_{\beta2}\end{bmatrix}&=\mathbf{Q}_2^\top\frac{1}{3}U_{\mathrm{dc}}\begin{bmatrix}2&-1&-1\\-1&2&-1\\-1&-1&2\end{bmatrix}\begin{bmatrix}S_{a2}\\S_{b2}\\S_{c2}\end{bmatrix}\\&=\mathbf{Q}_2^\top U_{\mathrm{dc}}\begin{bmatrix}S_{a2}\\S_{b2}\\S_{c2}\end{bmatrix}.\end{aligned} \tag{31}$$

The output voltage vectors of three-phase VSI driving the faulty winding are determined by the switch states (S_{n1}, S_{b1}, S_{c1}). The output voltage vector can be expressed in α–β plane using $\mathbf{D}_1\mathbf{Q}_1^\top$ in (5), i.e.,

$$\begin{aligned}\begin{bmatrix}u_{\alpha1}\\u_{\beta1}\end{bmatrix}&=\mathbf{D}_1\mathbf{Q}_1^\top=U_{\mathrm{dc}}\begin{bmatrix}-1&1&0\\-1&0&1\end{bmatrix}\begin{bmatrix}S_{n1}\\S_{b1}\\S_{c1}\end{bmatrix}\\&=\begin{bmatrix}3&0\\0&1\end{bmatrix}\mathbf{Q}_2^\top U_{\mathrm{dc}}\begin{bmatrix}S_{n1}\\S_{b1}\\S_{c1}\end{bmatrix}.\end{aligned} \tag{32}$$

Comparing (31) and (32), the only difference is that the α-axis component of the faulty three-phase VSI output voltage vector is scaled by 3. The all nonzero base

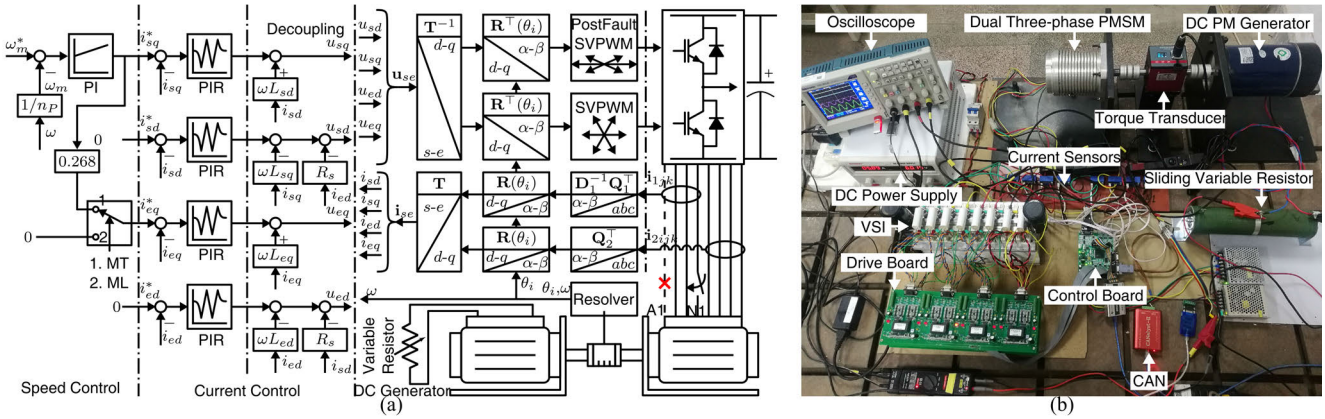

FIGURE 6. Overall postfault control scheme and picture of the experimental setup. (a) Overall postfault control scheme. PIR controllers used in (a) are shown in Fig. 3. (b) Picture of the experimental setup.

voltage vectors for all switch states are shown in Fig. 5. If the voltage vectors of faulty three-phase VSI is scaled by 1/3 along α-axis, they are completely coincides with the voltage vectors of the healthy three-phase VSI. Therefore, the conventional SVPWM can still to be used if the modulated voltage vectors is scaled by 1/3 along with α-axis.

The entire postfault FOC scheme for D3 SPMSM under single-phase OCF is depicted in Fig. 6 (a).

V. EXPERIMENTAL VERIFICATION

A. EXPERIMENTAL PROTOTYPE

In order to assess the feasibility and validity of the proposed control scheme under postfault operation, an experimentation has been conducted on a 350 W dual three-phase PMSM drive system. Fig. 6 (b) shows the experimental platform. The test bench is composed of a D3 SPMSM, two dual three-phase half-bridge VSIs with a single dc link, a PM dc generator as the load and a dc power supply. Single-phase OCF is emulated by directly disconnecting one of the motor phases, phase-1A, in the following results. The neutral point of the faulty winding (1N) is connected to the midpoint of the leg originally connected with phase-1A. The D3 PMSM is mechanically coupled with the torque transducer and the dc PM generator whose terminal is connected with a sliding variable resistor for load changing. The terminal voltage of the dc machine is used to estimate the shaft speed and output torque. The motor phase currents and rotor speed/position are measured with Hall-effect sensors and a resolver coaxially mounted inside the motor, respectively. SKMIKRON's IGBT modules SKM75GB128D are utilized as power devices with a switching frequency 10 kHz. CONCEPT's 2SD315AI are employed in IGBT drive circuits. The overall control algorithm is implemented on a digital signal processor (DSP) platform with TI's TMS320F28335. The control cycle is 100 us as the same as the sampling period of current, rotor speed and position angle. The waveforms were measured through voltage and current probes and recorded by the oscilloscope.

TABLE 1. Parameters of the D3 SPMSM drive.

Symbol	Quantity	Value
V_{dc}	DC bus voltage	60 V
ω_N	Rated rotor speed	1500 r/min
I_N	Rated phase current	3.5 A (RMS)
T_N	Rated torque	2 N·m
P_N	Rated power	350 W
R_s	Phase resistance	0.23 Ω
$L_{ls}+L_s$	Phase self-inductance	0.22 mH
L_m	Mutual inductance in the same winding	−0.14 mH
M_s	Mutual inductance of the same phases	0.07 mH
M_m	Mutual inductance of different phases	−0.03 mH
λ_{m1}	PM flux linkage	0.0745 Wb
λ_{m3}	PM third harmonic flux linkage	0.00398 Wb

The main parameters of the tested D3 SPMSM is listed in Table 1.

B. STEADY-STEADY PERFORMANCE UNDER HEALTHY AND FAULTY CONDITIONS

In order to verify the validity of proposed postfault FOC strategy, the steady state experiments have been firstly implemented under healthy and faulty conditions. The machine is driven in the speed mode and the speed reference is set to 1500 r/min. The load torque is 2 Nm proportional to the rotor speed.

Fig. 7 refers to the speed torque and current waveforms under, respectively, the healthy and phase-1A open-circuit faulty conditions. It can be seen from Fig. 7(a) that the phase currents under healthy condition are symmetrical and the maximum amplitude of phase currents is about 5 A. The conventional Clarke and Park transformations are used to obtain the d- and q-axis currents. The average value of q-axis currents are both 1 p.u., which means that the torque generated by two winding sets are balanced. Besides, the q-axis current ripples of the set-1 and set-2 are 0.28 and 0.26 p.u., respectively, which are both small under healthy operation. Fig. 7(a) also shows the current trajectory in α-β plane, the trajectory is noncircular and slightly distorted

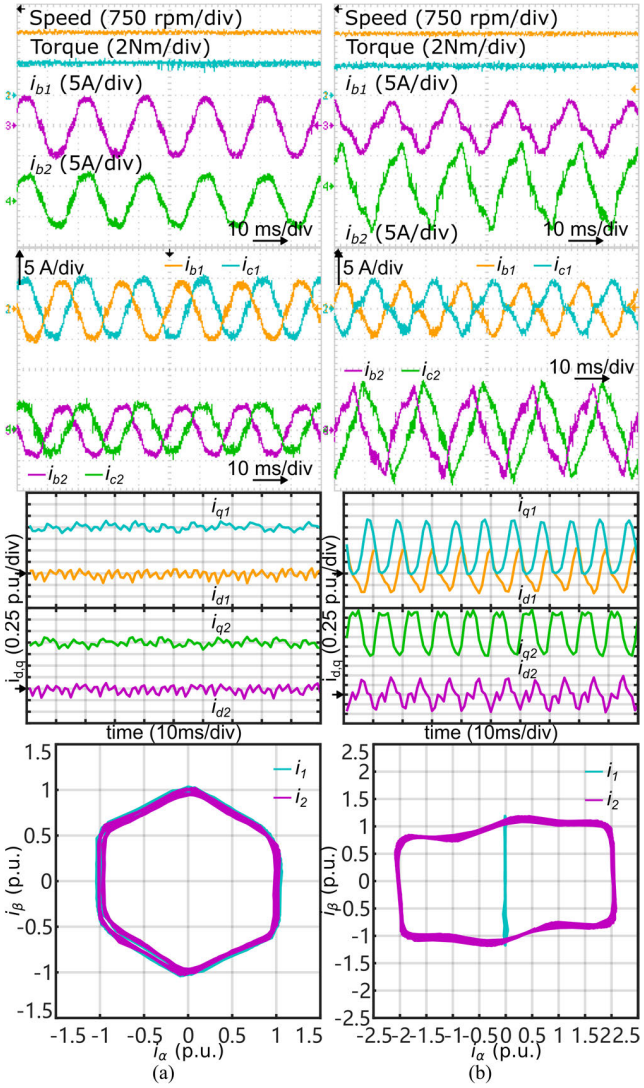

FIGURE 7. Experimental results at the steady state under healthy and faulty conditions from top to bottom: Speed, torque and phase currents, phase currents, currents in d-q frame, and current trajectories in $\alpha - \beta$ plane. (a) Healthy condition. (b) Faulty condition with phase-1A open-circuit.

because of the existence of little fifth harmonic currents. The fifth harmonic current suppression is out of the scope of this study.

Fig. 7(b) shows the steady-state performance under phase-1A open-circuit faulty condition with prefault control strategy. Thought the speed and torque under can be almost maintained as the same as these under the healthy condition, the phase currents of two winding sets are asymmetrical and seriously distorted. The average value of q-axis currents are 0.5 and 1.5 p.u., respectively and this means that the torque generated by two winding sets are unbalanced. In addition, the q-axis current ripples of the set-1 and set-2 are 1.19 and 1.21 p.u., respectively, which are much bigger than these under healthy condition. The d-axis current ripples of two winding sets are 1.03 and 0.94 p.u., respectively. The current trajectory under faulty condition is seriously distorted.

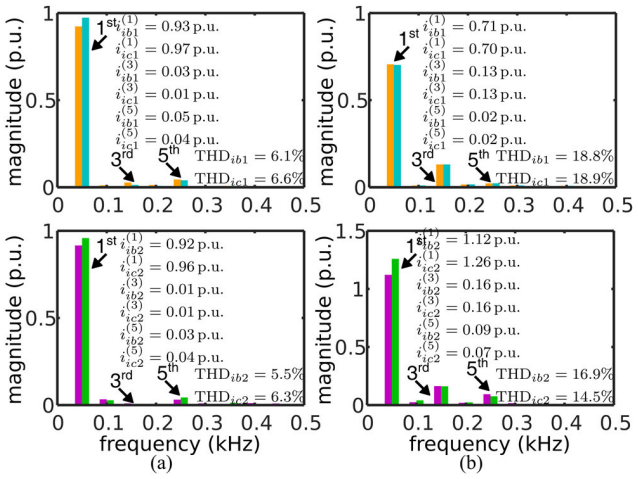

FIGURE 8. Frequency spectra of the phase currents at 1500 rpm. Figures from top to bottom are: Phase currents of winding set-1 and set-2. (a) Healthy condition. (b) Faulty condition with phase-1A open-circuit.

As can be seen, the current trajectory of set-1 is line due to the loss of phase-1A. Because of the closed-loop control scheme, the current trajectory of set-2 is actively distorted to provide the smooth total torque. Fig. 8 refers to the frequency spectra of the phase currents under healthy and faulty conditions. The main components of harmonic currents and total harmonic distortion (THD) are also given.

C. STEADY-STATE PERFORMANCE UNDER POSTFAULT CONTROL CONDITION

In order to investigate the current performance under both ML FOC and MT FOC after single-phase OCF, Steady-state experiments have been carried out. The machine is driven in the speed mode and the speed reference is set to 1500 r/min. The load torque is 2 Nm proportional to the rotor speed. The experimental current waveforms for ML/MT FOC schemes with and without PR controllers are presented in Fig. 9 (a), (b), (c) and (d). The d- and q-axis currents and current trajectories in α–β plane in Fig. 9 are obtained with the transformations in (7).

It can be seen from Fig. 9 that the ML FOC makes the q-axis component of currents with the equal average value,, while the MT FOC yields the phase currents with equal magnitudes. The phase currents of set-1 for the control schemes without PR controllers are seriously distorted as nonsinusoidal and the phase currents of set-2 are also slightly distorted due to the mutual inductance between two sets. The main component of phase current harmonics is third harmonic. Compared with the control schemes without PR controllers, the ones with PR controllers can significantly suppress the third order harmonics in both sets. Fig. 8 illustrates the frequency spectrum of the phase currents. It can be clearly observed that the large amount of third components of harmonics are noticeable reduced with PR controllers.

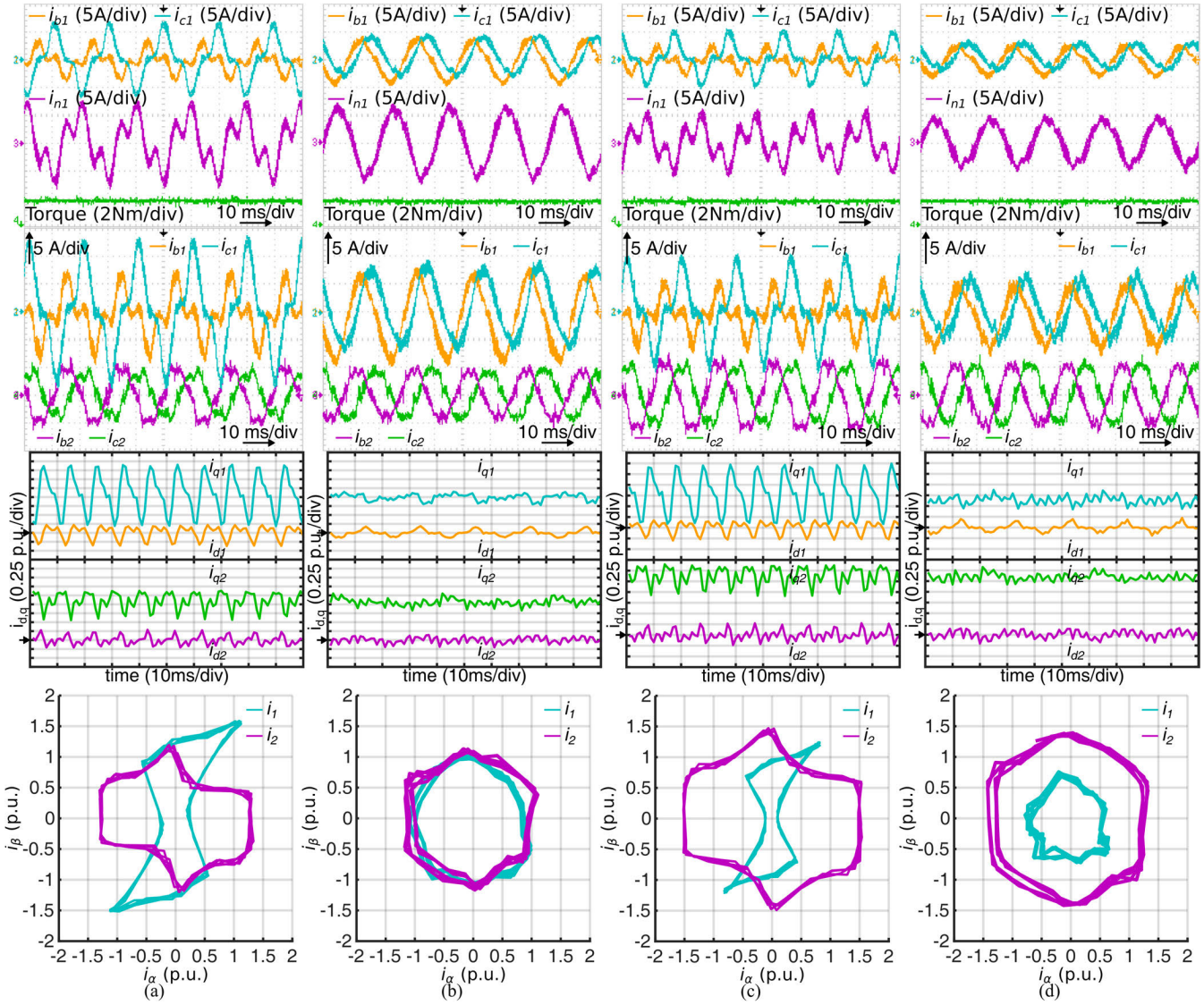

FIGURE 9. Experimental results at the steady state from top to bottom: Phase currents, currents in $d-q$ frame, and current trajectories in $\alpha-\beta$ plane. (a) ML without PR controllers. (b) ML with PR controllers. (c) MT without PR controllers. (d) MT with PR controllers.

It should be mentioned that little fifth harmonic currents still exist for the both FOC strategies with PR controllers, which is responsible for the slightly distorted trajectories in α–β plane from Fig. 9 (b) and (d). They only take over a minor part of all harmonic components and their suppression is beyond the scope of this paper. The total harmonic distortion (THD) and major low-order current harmonics are shown in Fig. 10.

D. DYNAMIC RESPONSE

The dynamic response experiment to speed reference change was carried out. The speed reference is set to 1500 r/min at the beginning, and is suddenly dropped to 600 r/min at the instant $t = 3$ s, and finally rose up to 1200 r/min at the instant $t = 6$ s. Fig. 11 shows dynamics of speed, torque and phase currents under healthy, postfault ML and postfault MT operations. It can be seen in Fig. 11 that the smooth transient and accurate tracking are achieved. Moreover, the speed and torque dynamic response waveforms under both postfault conditions have good agreement with these under healthy condition. This means that the speed and torque dynamic performances can be achieved under postfault conditions with the proposed postfault control strategy.

E. CHARACTERISTIC CURVES

The steady-state experiments were carried out to investigate the performance under different loads. The load torque is changed by sliding variable resistor connected with the dc generator. Fig. 12 shows the characteristic curves under various loads which are given in per-unit system. The estimated torque and copper loss under ML and MT FOC strategies are given.

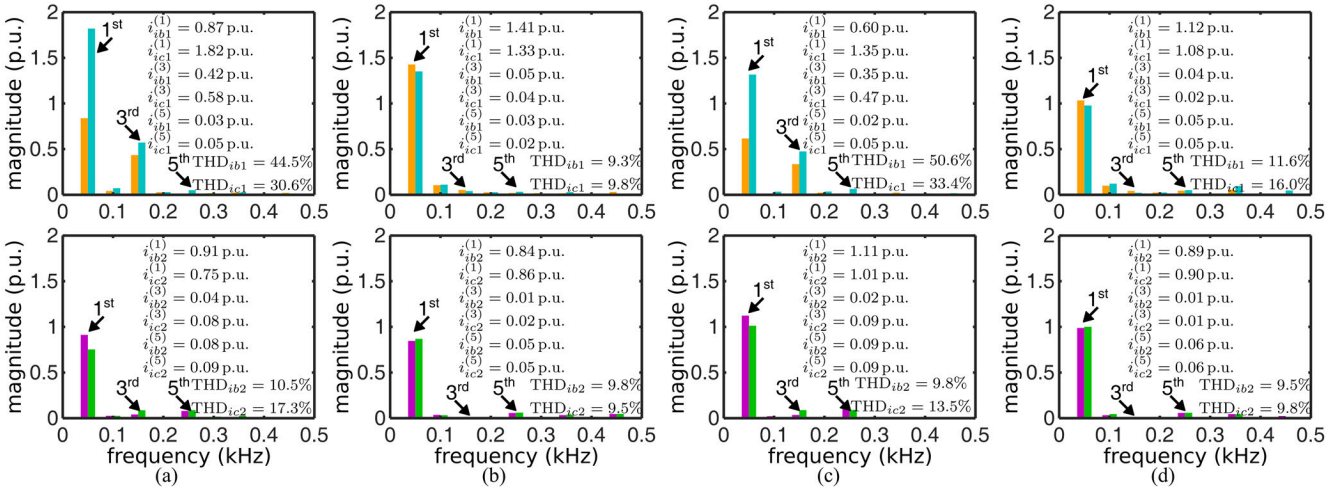

FIGURE 10. Frequency spectra of the phase currents at 1500 rpm. Figures from top to bottom are: Phase currents of winding set-1 and set-2. (a) ML without PR controllers. (b) ML with PR controllers. (c) MT without PR controllers. (d) MT with PR controllers.

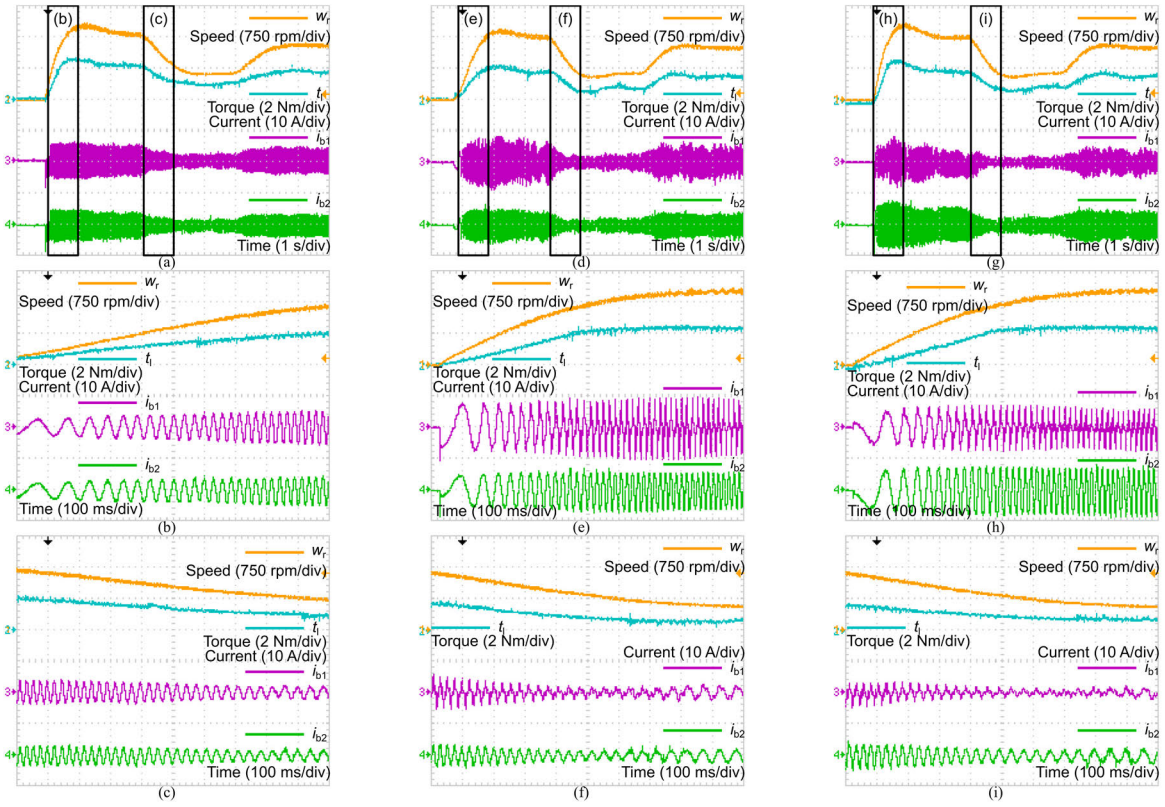

FIGURE 11. Speed and current dynamic response waveforms with healthy, ML and MT FOC strategies. (a)-(c) Healthy FOC; (d)-(f) ML FOC (g)-(i) MT FOC. (b)(e)(h). Zoom-in plot during rising transient. (c)(f)(i). Zoom-in plot during dropping transient.

VI. CONCLUSION

This paper proposed a postfault FOC strategy for the D3 SPMSM drive under single-phase OCF. A postfault decoupled model has been developed. Based on the proposed decoupled model, the entire postfault FOC strategies with ML and MT criteria were provided. PR controllers are employed to reduce the harmonic currents after fault occurs. Furthermore, the postfault SVPWM was also presented. The proposed postfault control strategies had been experimentally verified.

APPENDIX

DERIVATION OF POSTFAULT REDUCED-ORDER TRANSFORMATIONS

The postfault reduce-order transformation can be derived from base vector transformation. The base vector

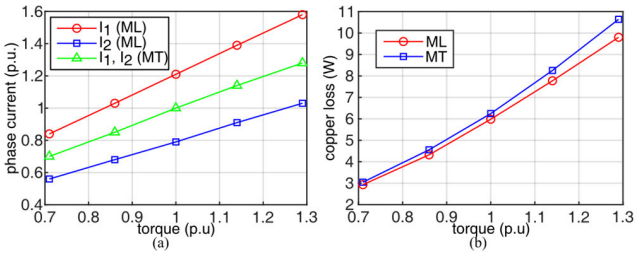

FIGURE 12. Characteristic curves. (a) Phase currents v.s. torque. (b) Copper loss v.s. torque.

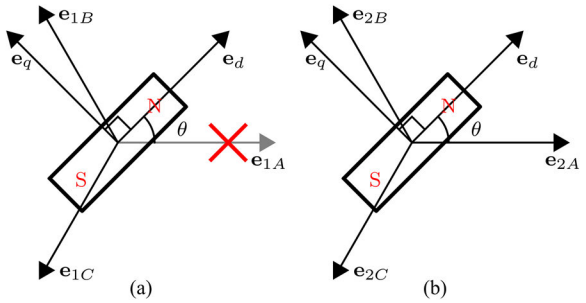

FIGURE 13. Relationship between the three-phase base vectors in abc frame and those in dq frame. (a) Faulty winding set-1 with phase-1A open-circuit. (b) Healthy winding set-2.

transformation is used to mapping the base vectors in *abc* frame into *dq* frame. Fig. 13 depicts the relationship between the base vectors of two three-phase winding, namely faulty set-1 with phase-1*A* open-circuit and healthy set-2 in *abc* and *dq* frame, respectively. From Fig. 13(a), the base vector transformation of faulty winding set-1 can be represented by the matrix $\mathbf{E}_F$ as follows,

$$\mathbf{E}_F = \begin{bmatrix} \mathbf{e}_{1b} & \mathbf{e}_{1c} \end{bmatrix} = \begin{bmatrix} \cos(\theta - \frac{2\pi}{3}) & \cos(\theta + \frac{2\pi}{3}) \\ -\sin(\theta - \frac{2\pi}{3}) & -\sin(\theta + \frac{2\pi}{3}) \end{bmatrix} \tag{33}$$

By using the singular value decomposition (SVD) technique, $\mathbf{E}_F$ can be decomposed as

$$\mathbf{E}_F = \mathbf{R}(\theta)\mathbf{D}\mathbf{Q}^\top \tag{34}$$

where

$$\mathbf{R}(\theta) = \begin{bmatrix} \cos\theta & \sin\theta \\ -\sin\theta & \cos\theta \end{bmatrix}, \quad \mathbf{D}_1 = \begin{bmatrix} \sqrt{3} & 0 \\ 0 & 1 \end{bmatrix},$$
$$\mathbf{Q}_1^\top = \sqrt{\frac{1}{2}} \begin{bmatrix} -1 & 1 \\ -1 & -1 \end{bmatrix}^\top$$

$\mathbf{R}(\theta)$ and $\mathbf{Q}_1^\top$ are orthogonal matrices and $\mathbf{D}_1$ is the diagonal matrix.

According to the relationship between base vector transformation and coordinate transformation, the current transformation mapping current vectors from *abc* frame to *dq* frame can be expressed as

$$\mathbf{T}_{1I}(\theta) = (\mathbf{E}_F^\top)^{-1} = \mathbf{R}(\theta)\mathbf{D}_1^{-1}\mathbf{Q}_1^\top \tag{35}$$

Based on the constant power constraint of the voltage and current transformations, i.e., $\mathbf{T}_U^\top(\theta)\,\mathbf{T}_I(\theta) = \mathbf{I}$, where $\mathbf{I}$ is the unity matrix, the voltage transformation can be derived as

$$\mathbf{T}_{1U}(\theta) = (\mathbf{T}_{1I}^\top(\theta))^{-1} = \mathbf{R}(\theta)\mathbf{D}_1\mathbf{Q}_1^\top \tag{36}$$

From Fig. 3(b), the base vector transformation of healthy winding set-2 can be represented by the matrix $\mathbf{E}_H$ as follows,

$$\begin{aligned} \mathbf{E}_H &= \begin{bmatrix} \mathbf{e}_{2a} & \mathbf{e}_{2b} & \mathbf{e}_{2c} \end{bmatrix} \\ &= \begin{bmatrix} \cos(\theta) & \cos(\theta - \frac{2\pi}{3}) & \cos(\theta + \frac{2\pi}{3}) \\ -\sin(\theta) & -\sin(\theta - \frac{2\pi}{3}) & -\sin(\theta + \frac{2\pi}{3}) \end{bmatrix} \end{aligned} \tag{37}$$

By using the singular value decomposition (SVD) technique, $\mathbf{E}_F$ can be decomposed as the classical Park and Clarke transformations, i.e.,

$$\mathbf{E}_H = \mathbf{R}(\theta)\mathbf{Q}_2^\top \tag{38}$$

where

$$\mathbf{Q}_2^\top = \sqrt{\frac{2}{3}} \begin{bmatrix} 1 & \frac{1}{2} & \frac{1}{2} \\ 0 & \frac{\sqrt{3}}{2} & -\frac{\sqrt{3}}{2} \end{bmatrix}$$

Therefore, the voltage and current transformations mapping voltage and current vectors from *abc* frame to *dq* frame can be expressed as

$$\mathbf{T}_{2U}(\theta) = \mathbf{T}_{2I}(\theta) = (\mathbf{E}_H^\top)^{-1} = \mathbf{R}(\theta)\mathbf{Q}_2^\top \tag{39}$$

REFERENCES

[1] E. Levi, R. Bojoi, F. Profumo, H. A. Toliyat, and S. Williamson, "Multiphase induction motor drives—A technology status review," *IET Electr. Power Appl.*, vol. 1, no. 4, pp. 489–516, Jul. 2007.

[2] E. Levi, F. Barrero, and M. J. Duran, "Multiphase machines and drives–revisited," *IEEE Trans. Ind. Electron.*, vol. 63, no. 1, pp. 429–432, Jan. 2016.

[3] F. Barrero and M. J. Duran, "Recent advances in the design, modeling, and control of multiphase machines—Part I," *IEEE Trans. Ind. Electron.*, vol. 63, no. 1, pp. 449–458, Jan. 2016.

[4] M. J. Duran and F. Barrero, "Recent advances in the design, modeling, and control of multiphase machines—Part II," *IEEE Trans. Ind. Electron.*, vol. 63, no. 1, pp. 459–468, Jan. 2016.

[5] M. Barcaro, N. Bianchi, and F. Magnussen, "Faulty operations of a PM fractional-slot machine with a dual three-phase winding," *IEEE Trans. Ind. Electron.*, vol. 58, no. 9, pp. 3825–3832, Sep. 2011.

[6] R. Kianinezhad, B. Nahid-Mobarakeh, L. Baghli, F. Betin, and G.-A. Capolino, "Modeling and control of six-phase symmetrical induction machine under fault condition due to open phases," *IEEE Trans. Ind. Electron.*, vol. 55, no. 5, pp. 1966–1977, May 2008.

[7] B. Tian, Q.-T. An, J.-D. Duan, D.-Y. Sun, L. Sun, and D. Semenov, "Decoupled modeling and nonlinear speed control for five-phase PM motor under single-phase open fault," *IEEE Trans. Power Electron.*, vol. 32, no. 7, pp. 5473–5486, Jul. 2017.

[8] H. S. Che, M. J. Duran, E. Levi, M. Jones, W.-P. Hew, and N. A. Rahim, "Postfault operation of an asymmetrical six-phase induction machine with single and two isolated neutral points," *IEEE Trans. Power Electron.*, vol. 29, no. 10, pp. 5406–5416, Oct. 2014.

[9] S. Dwari and L. Parsa, "Fault-tolerant control of five-phase permanent-magnet motors with trapezoidal back EMF," *IEEE Trans. Ind. Electron.*, vol. 58, no. 2, pp. 476–485, Feb. 2011.

[10] L. Cheng, Y. Sui, P. Zheng, P. Wang, and F. Wu, "Implementation of post-fault decoupling vector control and mitigation of current ripple for five-phase fault-tolerant PM machine under single-phase open-circuit fault," *IEEE Trans. Power Electron.*, vol. 33, no. 10, pp. 8623–8636, Oct. 2018.

[11] B. Tian, Q.-T. An, J.-D. Duan, D. Semenov, D.-Y. Sun, and L. Sun, "Cancellation of torque ripples with FOC strategy under two-phase failures of the five-phase PM motor," *IEEE Trans. Power Electron.*, vol. 32, no. 7, pp. 5459–5472, Jul. 2017.
[12] Z. Liu, Z. Zheng, and Y. Li, "Enhancing fault-tolerant ability of a nine-phase induction motor drive system using fuzzy logic current controllers," *IEEE Trans. Energy Convers.*, vol. 32, no. 2, pp. 759–769, Jun. 2017.
[13] D. Glose and R. Kennel, "Carrier-based pulse width modulation for symmetrical six-phase drives," *IEEE Trans. Power Electron.*, vol. 30, no. 12, pp. 6873–6882, Dec. 2015.
[14] W. N. W. A. Munim, M. J. Duran, H. S. Che, M. Bermudez, I. Gonzalez-Prieto, and N. A. Rahim, "A unified analysis of the fault tolerance capability in six-phase induction motor drives," *IEEE Trans. Power Electron.*, vol. 32, no. 10, pp. 7824–7836, Oct. 2017.
[15] A. G. Yepes, J. Doval-Gandoy, F. Baneira, and H. Toliyat, "Postfault strategy for dual three-phase machines with minimum loss in the full torque operation range under two open phases," in *Proc. IEEE Energy Convers. Congr. Expo. (ECCE)*, Sep. 2018, pp. 3380–3385.
[16] M. Barcaro, N. Bianchi, and F. Magnussen, "Six-phase supply feasibility using a PM fractional-slot dual winding machine," *IEEE Trans. Ind. Appl.*, vol. 47, no. 5, pp. 2042–2050, Sep. 2011.
[17] B. Vaseghi, N. Takorabet, J. P. Caron, B. Nahid-Mobarakeh, F. Meibody-Tabar, and G. Humbert, "Study of different architectures of fault-tolerant actuator using a two-channel PM motor," *IEEE Trans. Ind. Appl.*, vol. 47, no. 1, pp. 47–54, Jan. 2011.
[18] W. Zhang, D. Xu, P. N. Enjeti, H. Li, J. T. Hawke, and H. S. Krishnamoorthy, "Survey on fault-tolerant techniques for power electronic converters," *IEEE Trans. Power Electron.*, vol. 29, no. 12, pp. 6319–6331, Dec. 2014.
[19] H. Zhou, W. Zhao, G. Liu, R. Cheng, and Y. Xie, "Remedial field-oriented control of five-phase fault-tolerant permanent-magnet motor by using reduced-order transformation matrices," *IEEE Trans. Ind. Electron.*, vol. 64, no. 1, pp. 169–178, Jan. 2017.
[20] J. W. Bennett, B. C. Mecrow, D. J. Atkinson, and G. J. Atkinson, "Safety-critical design of electromechanical actuation systems in commercial aircraft," *IET Electr. Power Appl.*, vol. 5, no. 1, pp. 37–47, 2011.
[21] E. Jung, H. Yoo, S.-K. Sul, H.-S. Choi, and Y.-Y. Choi, "A nine-phase permanent-magnet motor drive system for an ultrahigh-speed elevator," *IEEE Trans. Ind. Appl.*, vol. 48, no. 3, pp. 987–995, May/Jun. 2012.
[22] A. G. Yepes, J. Doval-Gandoy, and H. Toliyat, "Improvement of postfault performance of multiphase drives in terms of operating region and stator copper loss," in *Proc. 44th Annu. Conf. IEEE Ind. Electron. Soc. (IECON)*, Oct. 2018, pp. 5819–5824.
[23] H. M. Eldeeb, A. S. Abdel-Khalik, and C. M. Hackl, "Postfault full torque–speed exploitation of dual three-phase IPMSM drives," *IEEE Trans. Ind. Electron.*, vol. 66, no. 9, pp. 6746–6756, Sep. 2019.
[24] F. Baneira, J. Doval-Gandoy, A. G. Yepes, O. López, and D. Pérez-Estévez, "Control strategy for multiphase drives with minimum losses in the full torque operation range under single open-phase fault," *IEEE Trans. Power Electron.*, vol. 32, no. 8, pp. 6275–6285, Aug. 2017.
[25] A. Mohammadpour, S. Sadeghi, and L. Parsa, "A generalized fault-tolerant control strategy for five-phase PM motor drives considering star, pentagon, and pentacle connections of stator windings," *IEEE Trans. Ind. Electron.*, vol. 61, no. 1, pp. 63–75, Jan. 2014.
[26] Y. Zhou, X. Lin, and M. Cheng, "A fault-tolerant direct torque control for six-phase permanent magnet synchronous motor with arbitrary two opened phases based on modified variables," *IEEE Trans. Energy Convers.*, vol. 31, no. 2, pp. 549–556, Jun. 2016.
[27] M. J. Duran, I. Gonzalez Prieto, M. Bermudez, F. Barrero, H. Guzman, and M. R. Arahal, "Optimal fault-tolerant control of six-phase induction motor drives with parallel converters," *IEEE Trans. Ind. Electron.*, vol. 63, no. 1, pp. 629–640, Jan. 2016.
[28] A. Gaeta, G. Scelba, and A. Consoli, "Modeling and control of three-phase PMSMs under open-phase fault," *IEEE Trans. Ind. Appl.*, vol. 49, no. 1, pp. 74–83, Jan. 2013.
[29] M. Tousizadeh, H. S. Che, J. Selvaraj, N. A. Rahim, and B.-T. Ooi, "Performance comparison of fault-tolerant three-phase induction motor drives considering current and voltage limits," *IEEE Trans. Ind. Electron.*, vol. 66, no. 4, pp. 2639–2648, Apr. 2019.
[30] M. Jones, S. N. Vukosavic, D. Dujic, and E. Levi, "A synchronous current control scheme for multiphase induction motor drives," *IEEE Trans. Energy Convers.*, vol. 24, no. 4, pp. 860–868, Dec. 2009.
[31] C. Xia, B. Ji, and Y. Yan, "Smooth speed control for low-speed high-torque permanent-magnet synchronous motor using proportional–integral–resonant controller," *IEEE Trans. Ind. Electron.*, vol. 62, no. 4, pp. 2123–2134, Apr. 2015.

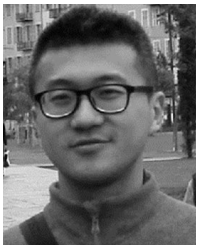

ZHE LIANG (Student Member, IEEE) received the bachelor's degree in electrical engineering from Xi'an Jiaotong University, Xi'an, China, in 2012, where he is currently pursuing the Ph.D. degree in electrical engineering with the School of Electrical Engineering.

His research interests include motion control, fault tolerant control, multiphase permanent magnet motor, and power electronics.

DELIANG LIANG (Senior Member, IEEE) received the B.S., M.S., and Ph.D. degrees in electrical engineering from Xi'an Jiaotong University, Xi'an, China, in 1989, 1992, and 1996, respectively.

Since 1999, he has been with the School of Electrical Engineering, Xi'an Jiaotong University, where he is currently a Professor. From 2001 to 2002, he was a Visiting Scholar with the Science Solution International Laboratory, Tokyo, Japan. His research interests include optimal design, control, and simulation of electrical machines, and electrical machine technology in renewable energy.

PENG KOU (Senior Member, IEEE) received the B.S. degree in electrical engineering and the M.S. and Ph.D. degrees in control science and engineering from Xi'an Jiaotong University, Xi'an, China, in 2005, 2008, and 2013, respectively.

From 2015 to 2016, he visited Ohio State University, Columbus, OH, USA. He is currently an Associate Professor with the School of Electrical Engineering, Xi'an Jiaotong University. His research interests include renewable energy, predictive control, microgrid, and power system optimization.

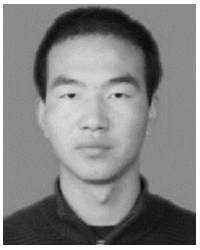

SHAOFENG JIA (Member, IEEE) was born in Shaanxi, China. He received the B.Eng. degree in electrical engineering from Xi'an Jiaotong University, Xi'an, China, in 2012, and Ph.D. degree in electrical engineering from the Huazhong University of Science and Technology, Wuhan, China, in 2017.

He is currently an Associate Professor with the School of Electrical Engineering, Xi'an Jiaotong University. He is the author/coauthor of about 50 IEEE technical articles. His research interests include design and control of novel PM and reluctance machines.